Inverse gas chromatography study of *n*-alkane and 1-alkene adsorption on pure-silica LTA (ITQ-29) and CHA

Niels De Witte[a], Sven Robijns[b], Joeri F.M. Denayer[a], Michiel Dusselier[b], Tom R.C. Van Assche[a*]

[a]Department of Chemical Engineering, Vrije Universiteit Brussel, Pleinlaan 2, 1050 Brussels, Belgium

[b]Center for Sustainable Catalysis and Engineering (CSCE), KU Leuven, Celestijnenlaan 200F, B-3001 Leuven, Belgium

[*]Corresponding author. E-mail address: tom.van.assche@vub.be.

Abstract

Inverse gas chromatography was used to investigate the Henry adsorption constants, adsorption enthalpies and entropies of *n*-alkanes and 1-alkenes up to C_{12} on the small-pore pure-silica zeolites LTA (ITQ-29) and CHA (Si-CHA). Small hydrocarbons with two adjacent single bonds (such as propane and 1-butene) are shown to experience strong mass transfer limitations due to the small pore window of these zeolites. In contrast, these mass transfer limitations were absent for hydrocarbons with alternating single- and double bonds (such as propylene and butadiene). The extent of this effect decreases with increasing carbon numbers on both zeolites. For Si-LTA, a typical monotonous increase in Henry constant with carbon number is observed for both *n*-alkanes and 1-alkenes. In contrast, a non-monotonous increase in Henry constants with carbon number, so-called cage (nestling) effect, is observed for Si-CHA. This effect is observed experimentally for 1-alkenes for the first time. Overall, our study sheds light on remarkable mass transfer limitations and cage effects that affect *n*-alkanes and 1-alkenes adsorption in these small-pore zeolites.

Introduction

Zeolites are microporous crystalline materials composed of tetrahedral units linked together through shared oxygen atoms, creating a network of channels and cavities with regularly sized rings, often referred to as pores. In a strict definition, 'zeolite' pertains specifically to the combination of alumina and silica tetrahedra. However, materials with pure silica or other substituted heteroatoms (e.g., P, Zn, Tn) in zeolitic frameworks are also commonly referred to as zeolites[1–3]. Depending on the connectivity of tetrahedral units, different three dimensional crystalline structures, so-called frameworks, can be defined. Zeolites can be characterized based upon their smallest pore size, and are typically divided into small-, medium- and large-pore zeolites[1]. Small-pore zeolites have 8-membered rings (8r) and are the smallest pore sizes through which hydrocarbons can diffuse in zeolites[1,4]. In contrast, medium- and large-pore zeolites have 10- and 12-membered rings respectively and allow for facile diffusion of linear hydrocarbons[5,6]. Zeolite CHA and zeolite LTA are well-known examples of small-pore zeolite frameworks. CHA zeolites consist of ellipsoid-shaped cages (6.8 x 10 Å)[7] interconnected by 8r pores of 3.8 Å x 3.8 Å[8] (Figure 1a). In LTA zeolites, the dimensions are larger than for the CHA zeolites, as LTA zeolites have spherical super-cages (α-cages) with a diameter of 11.4 Å[9], and have the largest 8r pores (4.1 Å x 4.1 Å)[8] of any small-pore zeolite (Figure 1b). In these small-pore zeolites, the close match between the size of the molecules and the pore windows strongly impacts adsorption, diffusion and catalytic conversion of molecules. This makes small-pore zeolites attractive catalysts and adsorbents for industrial applications such as methanol-to-olefins (MTO) conversion, direct CO_2 hydrogenation to olefins, and light gas separations[1,2,10–16].

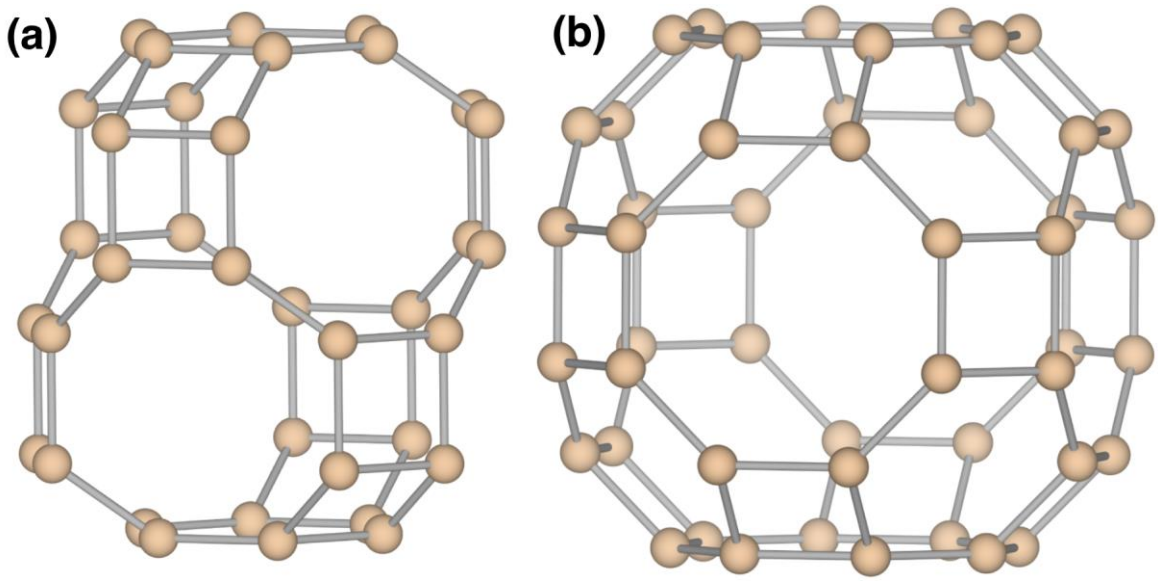


Figure 1: Schematic of the (a) CHA (t-cha) and (b) LTA (t-grc) zeolite cages.

In addition to the framework topology, the effective pore size of zeolites depends on the chemical composition of the framework and the extra-framework cations. By tuning the extra-framework cation content and type, the pore size can be tuned towards specific applications, as commonly applied in LTA type zeolites[17,18]. However, the chemical composition also alters the bond lengths, as a Si-O bond is smaller than an Al-O bond (1.61 Å vs 1.75 Å, respectively[10,17]).

Early synthesis of zeolite LTA and CHA were made using classic hydroxide media, yielding low silica-alumina (Si/Al) ratios up to 3[1]. These low Si/Al ratios limited the zeolite's usage in catalytic applications due to their low thermostability at high temperatures or under steam conditions[1,19]. More recent developments in synthesis have made high silica and pure-silica CHA and LTA zeolites possible[9,20–22]. In 1991, Zones[20] was able to synthesize CHA zeolites with higher Si/Al-ratio's (coined SSZ-13), which was soon followed by the first pure-silica CHA by the group of Camblor[21]. In 2004, Corma et al.[22] were the first to synthesize pure-silica LTA, commonly referred to as ITQ-29. Recently, the range between Si/Al 8 and pure-silica LTA was filled by the groups of Davis and Hong[9,23].

The effect of framework composition on the pore size is commonly exploited within the small-pore zeolite family to achieve kinetic separations of similar sized molecules[2,10,17,24,25]. Since the beginning of this century, Exxon Mobil[26–29] and Olson et al.,[30–32] have investigated and patented the usage of high-silica, pure-silica, and aluminophosphate variants of zeolites from various frameworks (CHA, ITE, DDR, ITW) for the kinetic separation of C_3 and C_4 isomers. By altering the framework composition, these materials obtain a smaller 8r pore window than their aluminosilicate zeolite variants, which can exclude similar-sized isomers. For example, pure-silica DDR allows for swift uptake of 1,3-butadiene and 2-trans-butene, while 1-butene and 2-cis-butene are excluded[33,34]. Ruthven and Reyes[10], among others[35,36], have highlighted that the minimum diameter of the pore window is the limiting factor for diffusion of adsorbates through 8r pore windows.

Molecular modelling studies have been used to investigate such adsorption and diffusion mechanisms in zeolites at the molecular level[37–46]. In these studies, pure-silica zeolites are commonly used as these lower the complexity of the force field, where cation location and mobility as well as the structural distribution of the Al do not have to be taken into account[47–51]. Ter Horst et al.[52] studied the passage of C_3- and C_4-isomers through the pore window (8r) of pure-silica DDR using molecular modelling. They reported that molecules with alternating single and double bonds, such as propylene and 1,3-butadiene, have a low activation energy for passing through the pore window. In contrast, molecules with successive single bonds, such as propane and 1-butene, have to substantially adjust their bond angle to pass through the pore window, increasing the energy barrier and diminishing their diffusion rate through the window.

Another remarkable phenomenon that has been studied using pure-silica zeolites, is the so-called ‘cage- and window effects’ in small-pore zeolites[38,53]. In a series of detailed computational studies, Dubbeldam et al.[38,54,55] elaborate on the existence of a non-monotonic variation of the Henry and diffusion constants with carbon number for *n*-alkanes in CHA, ERI and LTA frameworks. Generally, adsorption and diffusion properties of *n*-alkanes are

monotonically chain-length dependent[56–58]. However, for small-pore zeolites in which the pore system consists of cages connected through narrow pores (sometimes called windows), an unusual and controversial non-monotonic chain-length dependence behaviour is reported[59–63]. Here, increasing the chain length forces the molecule to coil up, or, once the chain-length becomes too long, protrude the pore window into the adjacent cage[38,59,64]. This incommensurate fit between adsorbate and adsorbent is proposed to lower their adsorption strength and increase their diffusion rate throughout the zeolite. The term 'window effect' was presented by Gorring in the context of non-monotonic diffusion coefficients, offering a 'window of increased transmittance' at higher carbon numbers, also linked to catalytic performance. Unfortunately, the term 'window effect' may be easily confused with the concept of 'a window' between cages, offered by 8r. On the other hand, 'cage-effects' have been used for unusual catalytic effects[53] or adsorption trends[59].

These effects are mostly studied computationally on pure-silica zeolites using *n*-alkanes as probe molecules[37,38,65]. Gorring[66] was the first to report on the existence of possible 'window effects' in zeolites based on uptake experiments, focusing on diffusion coefficients. However, these kinetic experiments are disputed due to non-linearity and non-isothermal artifacts[67,68]. Nevertheless, more recent experimental studies[58,60,68] using techniques as NMR show a non-monotonous decrease of the diffusion coefficient. Beyond these kinetic 'window' effects, non-monotonic equilibrium effects have only been experimentally confirmed on a polar LTA zeolite (Si/Al 1.0), a polar CHA zeolite (Si/Al 2.5) and on the iso-structural SAPO-34 using *n*-alkanes[59,69], but not using pure-silica variants, as typically employed in simulation studies. Such fundamental adsorption effects have been predicted for other, more reactive, chemical groups as alkenes[37] yet have not been reported experimentally, despite the higher relevance of such olefins as base and platform chemicals.

Despite the limited experimental data, a discrepancy may be noticed between the experimental and computational results on cage effects. The few experimental results on pure-silica CHA (Si-CHA) are limited up to carbon number 4 and show the strong kinetic hinderance

of hydrocarbons with two successive single bonds (such as propane and *n*-butane) leading to strongly reduced diffusion rates for these components[26,31,70]. These reports seem to suggest that adsorption measurements of large hydrocarbons will be experimentally challenging due to the strongly reduced diffusion rates. In contrast, computational studies report adsorption properties of *n*-alkanes on Si-CHA up to carbon number 16[37,38,54,55]. This observation poses the question if it is possible to experimentally measure the adsorption properties of long chain hydrocarbons within a practical timescale.

In this work, we present the unreported adsorption properties of *n*-alkanes, and the far less probed 1-alkenes, on Si-CHA and Si-LTA (ITQ-29), up to C_{12} using inverse gas chromatography (IGC). Using IGC, we first highlight the experimental difficulties of measuring the adsorption properties of smallest ($<C_6$) hydrocarbons on pure-silica small-pore zeolites due to mass transfer limitations. Subsequently, we report Henry constants, adsorption enthalpies and entropies with focus on large hydrocarbons ($>C_5$), revealing a cage-effect for CHA. In this work we will use the general term 'cage effect' for the non-monotonic adsorption behaviour with carbon number, focusing on the Henry coefficients and equilibria (and not kinetics). Finally, these values are compared to available modelling predictions.

Materials and methods

Zeolite synthesis

For the synthesis of pure-silica LTA (ITQ-29), the organic structure-directing agent (OSDA) 1,2-dimethyl-3-(4-methylbenzyl)imidazolium hydroxide (DMMBIOH) was prepared according to the method described by Kang et al.[71] The corresponding pure-silica LTA seeds were obtained through the modified recipe of Boal et al.[9] The pure-silica CHA was synthesized using a seed assisted fluorine route similar to the one described by Camblor et al.[21] Details on the synthesize of DMMBIOH, Si-LTA and Si-CHA are provided in the Supporting Information.

Zeolite characterization

The structures and purity of the OSDA were analysed and validated by hydrogen nuclear magnetic resonance (H-NMR). Powder X-ray diffraction (PXRD), nitrogen physisorption and scanning electron microscopy (SEM) were applied to characterize and validate the synthesis of zeolites Si-LTA and Si-CHA. Additional information on the techniques and experimental conditions can be retrieved in the Supporting Information.

Inverse gas chromatography

Inverse gas chromatography (IGC) was used to characterize the adsorption properties of molecules at zero coverage. The experiments were performed on a modified HP 6890 gas chromatograph (GC) system equipped with an external Bronkhorst mass flow controller, an external Gefran pressure transducer and a flame ionization detector (FID). The FID sample rate was set at 20 Hz. Gaseous components were manually injected using a Hamilton CR-700 20 µl syringe with a 0.1 µl resolution. Liquid components were automatically injected using an Agilent 7683 injector equipped with a 0.5 µl syringe with a 0.01 µl resolution. Statistical first moments μ_1 were calculated by integration of the peaks after baseline correction using the Agilent's ChemStation (B.04.03) software.

The adsorbent was prepared by compressing it into small disks, breaking them up, and sieving them to obtain 500-630 µm pellets (Figure S6). These pellets were loaded into a stainless steel Swagelok column with an inner diameter of 0.216 cm and outer diameter of 3.18 mm, with a length of 14.9 cm. The column was activated in situ under a constant flow of helium to a temperature of 350°C at a rate of 1°C/min and left at that temperature overnight.

For the IGC experiments, single components were injected into the column at a specific temperature and flow rate, and the first moment of the peak was monitored. An injection volume of 0.1 µl was used for gaseous hydrocarbons and 0.01 µl for liquid hydrocarbons. The supplier and purities of all hydrocarbons are provided in Table S1. The linearity of the isotherm was checked by varying the injection volume (Figure S10 and S11), and the first moment was found to be independent of the injection volume, indicating that the experiments were

performed in the Henry regime. The experiments were repeated several times in a time span of six months and confirmed the reproducibility of the experiments and the stability of the samples. To avoid any influence of dead volume or axial dispersion, experimental conditions were set such that the first moment was between 0.5 and 60 minutes. The Henry (adsorption) constants were calculated using Equation 1[59,72]:

$$\mu = \frac{L}{v_f}[(\varepsilon_{ext} + \varepsilon_{macr}) + (1 - \varepsilon_{ext} - \varepsilon_{macro})RT_{column}\rho_c K'] \quad \textbf{Eq. 1}$$

Where μ is the first moment corrected for the equipment dead time (s), L is the column length (m), v_f is the average superficial gas velocity (m/s), ε_{ext} is the external porosity (-), ε_{macr} is the macroporosity (-), R is the gas constant (J/mol/K), T_{column} is the column temperature (K), ρ_c is the crystal density (kg/m^3), and K' is the Henry adsorption constant (mol/kg/Pa). The crystal density ρ_c of each sample was calculated based upon the crystal structure of the IZA database[8].

The temperature dependency of the Henry's constants is described by the van't Hoff equation (Equation 2)[72], which allows for determination of the adsorption enthalpy and pre-exponential factor at zero coverage.

$$K' = K'_0 \, e^{\left(-\frac{\Delta H_0}{RT}\right)} \quad \textbf{Eq. 2}$$

Where K'_0 is the pre-exponential factor at zero coverage (mol/kg/Pa), and ΔH_0 is the adsorption enthalpy at zero coverage (J/mol). The adsorption entropy at zero coverage $\Delta S^{\theta}_{0,local}$ was calculated using Equation S1 and by use of a localized adsorption model (see Supporting Information for details). The adsorption enthalpy and entropy was obtained by linear regression on all the available measurements, taken at multiple flowrates and temperatures, for a single component.

To quantitively asses peak tailing in chromatograms, the tailing factor (T_f) was calculated following the United States Pharmacopeia (USP) recommendations[73] at 5% peak height using Equation 3:

$$T_f = \frac{a + b}{2a} \qquad \textbf{Eq. 3}$$

Where a is the distance from the leading peak edge to the middle point of the peak (*i.e.* the perpendicular of the highest point of the peak) at 5% of the peak height (s), and b is the distance from the trailing peak edge to the middle point of the peak at 5% peak height (s). Perfectly Gaussian shaped peaks result in T_f- values of 1. T_f-values below or above 1 indicate fronting or tailing of the peak, respectively.

Results & discussion

1. Adsorption and diffusion of small *n*-alkanes and 1-alkenes

In each IGC experiment, a small pulse of a single component is introduced, and the retention time of the peak is recorded. This allows to calculate the Henry constant of that component at the controlled column temperature (Equation 1). Under a given set of experimental conditions, the retention time depends on the adsorption equilibrium of the molecule for the zeolite.

In contrast, peak broadness, whether symmetric or asymmetric, can have numerous origins. These include axial dispersion and diffusion hinderance into the zeolite (Figure S8-S9), but also non-linear equilibrium adsorption[72], among other factors[74–76]. In this work, the column packing was optimized using a narrow particle size distribution (500-630 µm, Figure S6), and the linearity of the adsorption equilibrium was verified (Figure S10-S11). However, some degree of peak tailing still persists in our IGC experiments.

Figure 2a shows a typical chromatogram of ethane and ethylene (at 40°C) on Si-CHA, where Gaussian-like peaks with a limited amount of peak tailing are observed. Ethane has a higher

affinity for the Si-CHA zeolite than ethylene, as the former elutes later. In this pure-silica structure, the adsorptive interactions are dominated by van der Waals dispersive forces[36,77]. As a result, the *n*-alkane molecule interacts more strongly than the alkene of the same carbon number due to the additional hydrogen atoms.

For propylene, a similar retention time than ethane is observed (Figure 2a), but it should be stressed that this chromatogram was obtained at higher temperature (90°C), as the adsorption of propylene is stronger. Tailing of the ethane, ethylene and propylene peaks can likely be attributed to the axial dispersion and non-uniform packing of the adsorbent in the column, although other mechanisms can not be excluded.

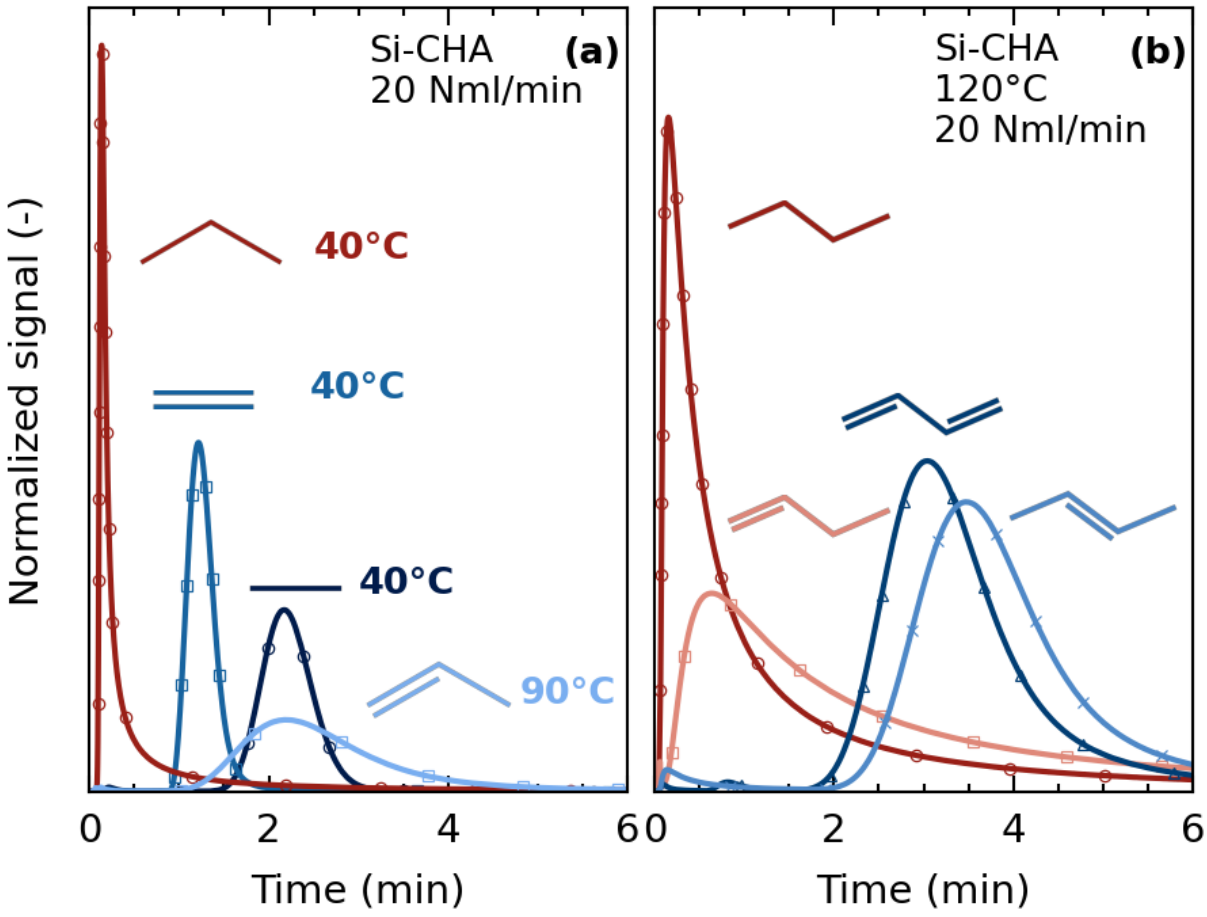


Figure 2: Chromatograms of C_2-C_4 *n*-alkanes and alkenes on Si-CHA at a flow rate of 20 Nml/min: (a) C_2- and C_3-isomers (ethane, ethylene, propane and propylene) at different temperatures, (b) C_4-isomers (*n*-butane, 1-butene, 1,3-butadiene, and 2-trans-butene) at 120°C.

Interestingly, and in contrast to ethane, ethylene and propylene, a completely different behaviour (Figure 2a) is observed for propane. The peak elutes immediately, almost coinciding with the dead time of the column, independent of the experimental temperature or flowrate (Figure S12).

Similar behaviour is observed for C_4-isomers where *n*-butane and 1-butene elute swiftly and their peaks have substantial tailing, while 1,3-butandiene and 2-trans-butene give rise to Gaussian-like peaks (Figure 2b and S13). Injections of *n*-pentane lead to smeared-out peaks, and the peaks are influenced by temperature and flowrate, as can be seen in Figure 3a. The temperature and flowrate dependency suggest that *n*-pentane is adsorbing within the timescale of our experiments, but faces more pronounced mass transfer limitations.

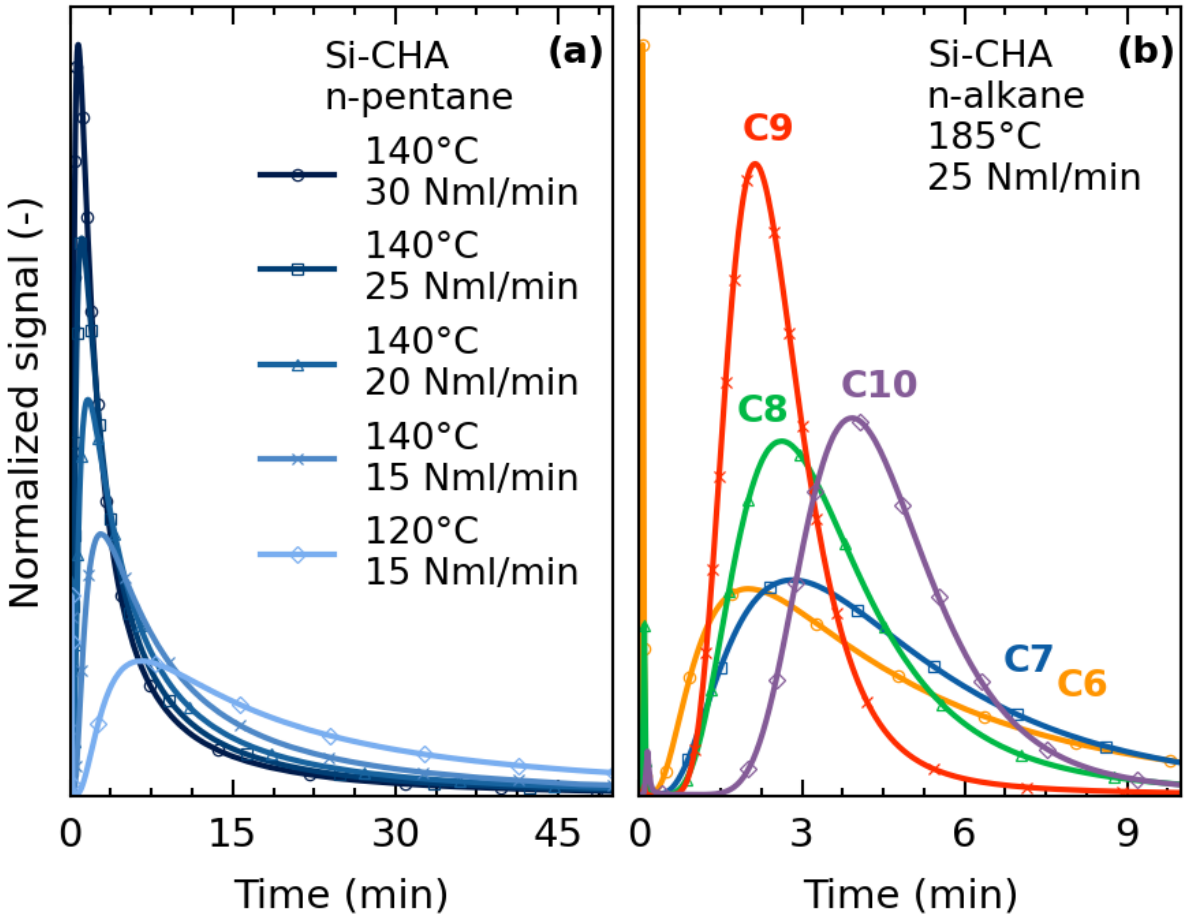


Figure 3: Chromatograms of different *n*-alkanes on Si-CHA: (a) *n*-pentane at various experimental conditions, (b) *n*-alkanes (C_6-C_{10}) at 180°C and 25 Nml/min.

This observed behaviour can be rationalized. As previous studies have pointed out, small hydrocarbon molecules with two adjacent single bonds (such as propane) experience strong steric hinderance when diffusing through the 8r pore window[31,33,34,36,52,70], as three adjacent CH_x ($x = 2\ or\ 3$) groups experience repulsive interactions of the silica tetrahedrons when passing through the pore window. Using IGC, this substantial mass transfer resistance can be assessed qualitatively, as fast-diffusing molecules give rise to Gaussian-like peaks, while slow diffusing molecules result in (almost) immediate eluting and smeared-out peaks for these components. The latter components are not in equilibrium with the adsorbent, due to their slow diffusion throughout the zeolite, and thus making accurate Henry constant determination impossible within our experimental conditions range.

Simulations by Ter Horst et al.[52] have found no significant changes in bond lengths and torsions, and only changes in bond angle when propane is passing through the 8r pore window of DDR zeolite. Similar behaviour for the 8r pore window of Si-CHA can be expected, as Si-CHA's pore window only deviates slightly from the Si-DDR pore window (3.6 Å x 4.4 Å)[8]. The fast uptake of components with more linear shape is confirmed using 1,3-trans-pentadiene, a C_5-isomer, in which double bonds alternate with single bonds giving rise to a linear molecular shape. Injection of 1,3-trans-pentadiene gives rise to a Gaussian peak (Figure S14), confirming this behaviour, in contrast to the non-linear shaped *n*-pentane in Figure 3a.

Remarkably, injections of longer *n*-alkanes and 1-alkenes lead to peaks with a more Gaussian peak shape, as seen in Figure 3b and S15, respectively. This observation suggests that large components diffuse more easily through the pore window than the smaller components. To avoid ambiguity, the quality of the peaks was also quantified using the tailing factor (Equation 3), confirming that of peak quality improves with higher carbon number, as peak tailing

decreases substantially from *n*-pentane to *n*-heptane (Figure S16). The molecular study by Dubbeldam et al.[38] offers to rationalize these findings. Their work predicted that the energy barrier for passing the 8r pore window substantially lowers for larger *n*-alkanes compared to propane. In the case of propane, all three CH_x groups experience the repulsive interactions of the pore window. Additional CH_x groups of longer molecules will occupy more favourable position away from the pore window[38]. Consequently, the energy barrier for passing the pore window decreases with increasing carbon number. The macroscopic IGC technique does not allow to reveal the details of such mechanisms. Larger carbon numbers are typically associated with smaller diffusion coefficients, potentially restricting access to the inner cages with adsorption occurring solely on the outer surface of the crystals. However, based on experiments with varying injection volume (Figure S10), these effects are considered unlikely here.

Shifting attention to Si-LTA, similar behaviour is observed as for Si-CHA. Chromatograms of propane, *n*-butane show similar strong peak widening and peak tailing, while molecules with alternating single and double bonds give rise to Gaussian-like peaks (Figure S17-S20). Similar to Si-CHA, the peak shapes also become more Gaussian-like with increasing carbon number (Figure S21). While Si-LTA has a slightly larger pore window than Si-CHA (4.1 Å and 3.8 Å[8], respectively), its pore window still seems to cause steric hinderance for small hydrocarbons.

2. Determination of Henry adsorption constants

The Henry adsorption equilibrium constants provide a measure for both the adsorption strength (adsorption enthalpy) of the adsorbate on the adsorbent and the loss of freedom (adsorption entropy) at given temperature and zero coverage. As discussed above, the Henry constants of slowly diffusing C_3- and C_4-isomers on Si-CHA and Si-LTA cannot be determined under our experimental conditions. Starting from C_5, the peak quality gradually improves, which allows to determine the first moment (i.e. mean retention time) of the peak, which can be used to calculate the Henry constants (Equation 1). However, extensive tailing is still

undesired as it severely affects the accuracy of the first moment, due to the uncertainty of the end point of the peak.

Chromatographic theories, such as the van Deemter equation[78], state that the width of the peak is dependent on the applied gas flowrate through the column. However, according to Equation 1, the Henry constant should be constant regardless of the applied flowrate during the experiments, or to put differently, the product of the first moment and superficial velocity ($\mu * v_f$) should remain constant. Given the possible severity of the peak tailing on Si-CHA and Si-LTA, the Henry constant measurements where conducted at multiple flowrates to verify the applicability of Equation 1.

Figure 4 shows the logarithm of the apparent Henry constants in function of inverse temperature for *n*-alkanes (C_5-C_{12}) on Si-CHA at different flowrates. The apparent Henry constant values are obtained by applying Equation 1 on the obtained data, even under invalid flowrate affected conditions. Only when the apparent Henry constant values are independent of the flowrate, is the apparent Henry constant equal to the Henry constant. However, this is not the case for *n*-pentane and *n*-dodecane, where the apparent Henry constant values differ significantly with flowrate (at various temperatures), possibly due to mass transfer limitations. Consequently, Henry constants cannot be calculated for these components. In contrast, variation of the gas flowrate does not alter the apparent Henry constant values for C_6-C_{11}, thus allowing for correct Henry constants determination, as these measurements were taken at equilibrium in absence of mass transfer limitations (Figure S28). Among the 1-alkenes, 1-pentene is also excluded due to clear flowrate dependency (Figure S23). Hence, in the rest of the work we will mostly focus on the adsorption equilibria (not kinetics) of C_6-C_{11} *n*-alkanes and 1-alkenes.

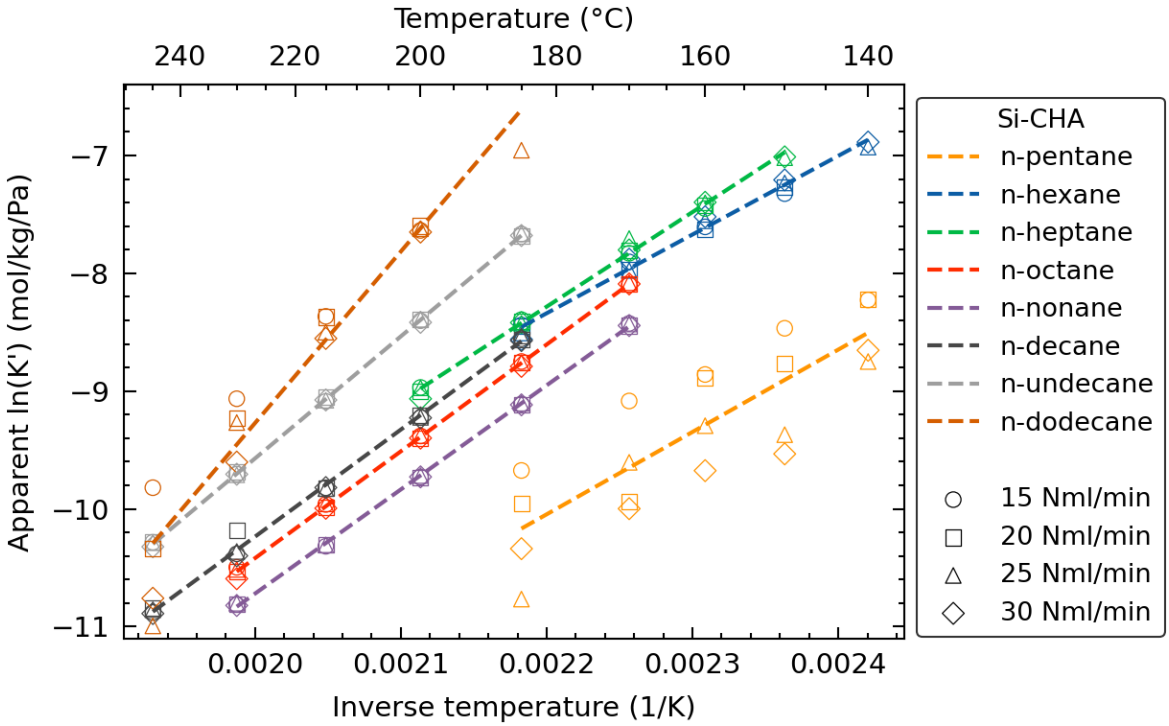


Figure 4: Natural log of the apparent Henry constant K' in function of inverse temperature for *n*-alkanes with carbon number 5-12 on Si-CHA. Symbols correspond to the flowrate during the experiment. Linear regression is performed on the complete dataset for each component and depicted by the dashed lines. R^2 was greater than 0.99 for all components, except for C_5 and C_{12}.

Figure 4 represents the van't Hoff plot for components C_6-C_{11}, where no flowrate dependency exists. Remarkably, the Henry constant at a given temperature do not rise monotonically with carbon number, termed 'cage effect' in this work. For example at 185°C the order of (apparent) Henry constant values is $C_5 < C_9 < C_8 < C_{10} < C_6 < C_7 < C_{11} < C_{12}$. Figure 5 illustrates the variation of Henry constants for *n*-alkanes and 1-alkenes on Si-CHA and Si-LTA with carbon number at 185°C, and highlights this unusual variation of the Henry constants. Typically, a linear trend is observed for zeolites[56,57], as each CH_x group added to the chain increases interactions between the adsorbate and the zeolite. However, on Si-CHA, the logarithm of Henry constants exhibits a remarkable non-monotonic behaviour, showing a increase until carbon number 6 followed by a local minimum at carbon number 9, after which an (apparently linear) increase is observed again. Such an effect has also been reported for the adsorption

of *n*-alkanes on a polar CHA-type zeolite[59], yet such a non-linear effect has not been reported experimentally for 1-alkenes on any small-pore zeolite before. This observation confirms that other types of molecules, besides *n*-alkanes, also experience cage nestling effects.

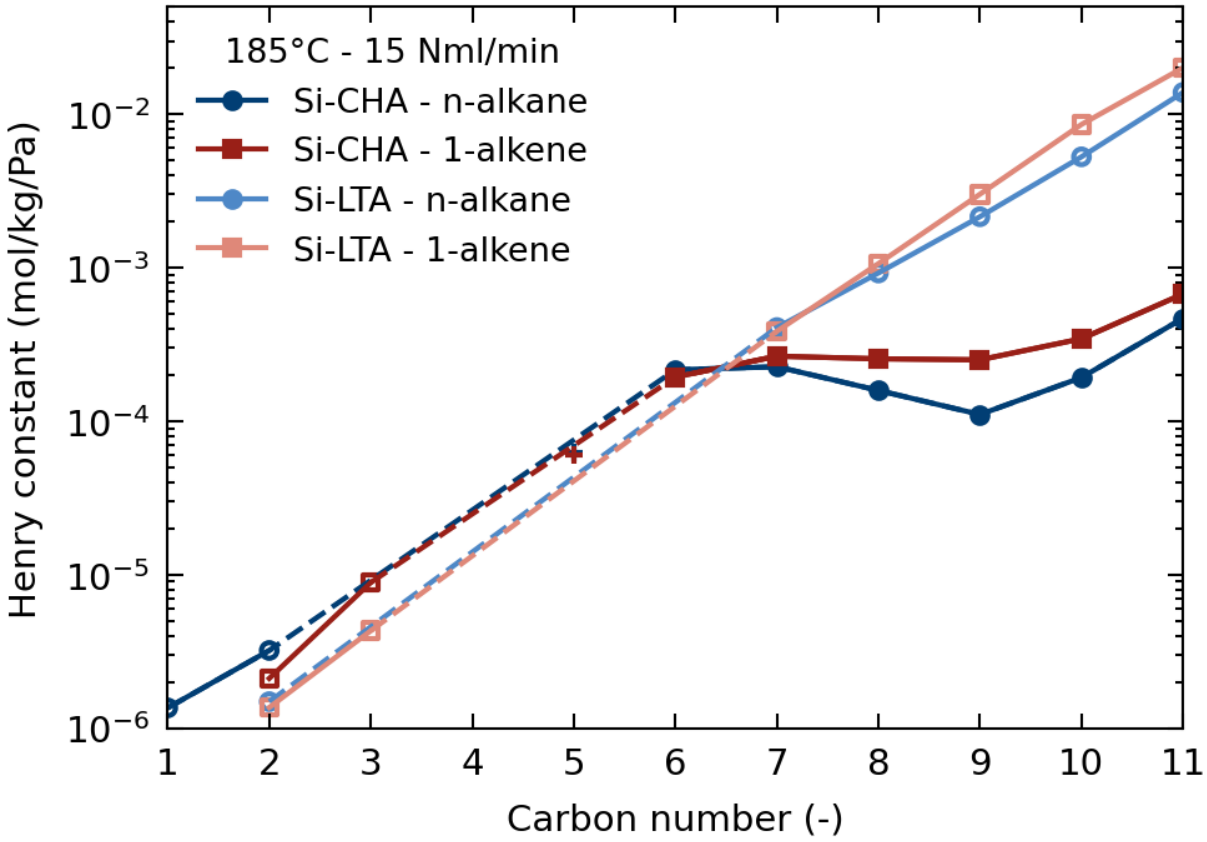


Figure 5: Henry constants in function of the carbon number for *n*-alkanes and 1-alkenes on Si-CHA and Si-LTA at 185°C and 15 Nml/min. Henry constants of C_5-isomers on Si-CHA are depicted by a plus marker to give an indication of its value, but these values are not true Henry constants due to their flowrate dependency. Dashed lines are added to guide the eye and compensating for missing data due to mass transfer limitations.

For *n*-alkanes, such cage effect has been studied before, where previous studies have suggested that *n*-pentane can still fit in an optimal all-trans configuration inside of the CHA cage[15,38,59]. However, larger molecules have to deviate from this all-trans configuration in order to fit inside the cage, introducing repulsive interactions and lowering their spatial freedom.

Once the chain becomes too big for the cage, it will protrude the pore window into the adjacent cage[38,59,64] (Figure 6). For the less studied 1-alkenes, the local minimum observed here at C_9 appears to be less substantial, with the Henry constants of C_7 to C_{10} having similar values.

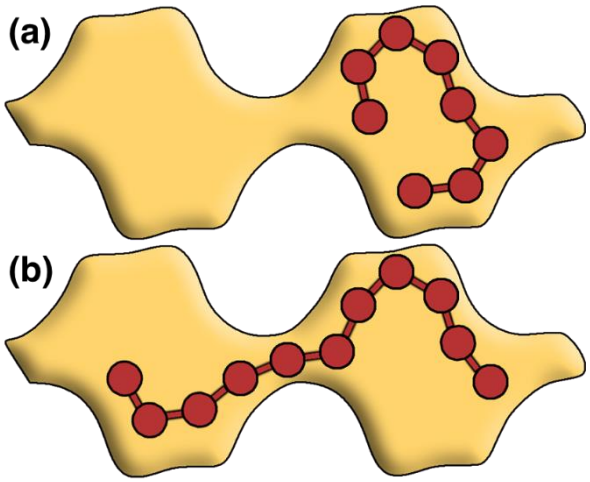


Figure 6: Schematic of the *n*-alkanes adsorption mechanism in two adjacent CHA-cages. (a) Adsorption of *n*-octane in a coiled-chain configuration within one cage. (b) Adsorption of *n*-undecane by protruding the pore window between two adjacent CHA-cages.

In contrast to Si-CHA, a linear increase of the logarithm of the Henry constants with increasing carbon number is observed for both *n*-alkanes and 1-alkenes on Si-LTA from C_6 on, being a more common observation for zeolites. The Henry constants of 1-alkenes and *n*-alkanes on Si-LTA do not differ much, as the van der Waals interactions are similar for both homologous series. Cage nestling effects, as seen on Si-CHA, are anticipated for Si-LTA as well, but due to the size of the LTA super-cage these effects should only be noticeable from carbon number 18 and above[37,38,69], outside our experimental accessible range.

3. Thermodynamic analysis

The adsorption enthalpy and entropy contributions can be calculated by linearizing the van't Hoff plots using Equation 2 and Equation S1 (assuming a localized adsorption model). This allows to gain a more detailed understanding of the adsorption process. Figure 7 shows the

adsorption enthalpy and entropy on Si-LTA for *n*-alkanes and 1-alkenes, which showed a linear trend in Figure 5. Both homologous series also show a typical linear increase in adsorption enthalpy and entropy with carbon number[56,57,79–81]. Remarkably, the 1-alkene series has slightly higher values for both quantities compared to *n*-alkanes.

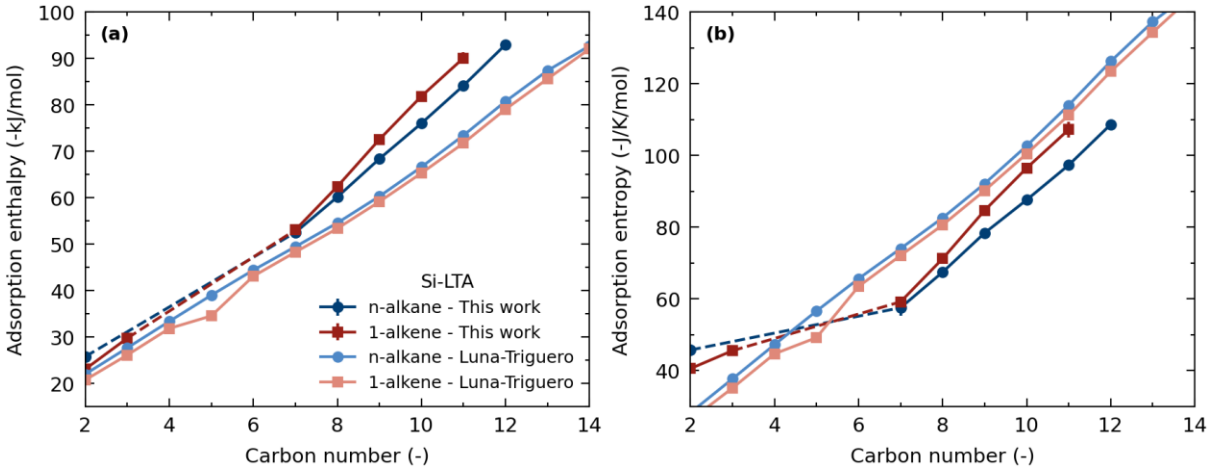


Figure 7: (a) Adsorption enthalpy and (b) adsorption entropy at zero coverage in function of the carbon number for *n*-alkanes and 1-alkenes experimentally obtained in this work (Si-LTA) and by Luna-Triguero et al.[37] via simulations (Si-LTA). Dashed lines are added to enhance the visualization and compensating for missing data due to mass transfer limitations. Standard deviation is given for *n*-alkane and 1-alkene series of this work.

The interactions of *n*-alkanes and 1-alkenes with the zeolite are weak van der Waals interactions, where enthalpic contributions are offset by entropic contributions. Each additional carbon adds two hydrogen atoms that can have van der Waals interactions with the zeolite, increasing the adsorption enthalpy. Likewise, each additional interaction lowers the degrees of freedom of the adsorbate, increasing the adsorption entropy. This effect, often referred to as the enthalpy-entropy compensation, is a general property of weak intermolecular interactions[82].

The experimentally obtained adsorption enthalpies and entropies on Si-LTA are compared to computational results by Luna-Triguero et al.[37] in Figure 7. For lower carbon numbers (C_2-C_5),

the adsorption enthalpies compare reasonably well. Interestingly, for the higher carbon numbers, the experimental adsorption enthalpy and entropy values deviate slightly from the simulations. The higher adsorption enthalpies combined with the lower adsorption entropies in this work result in higher Henry constants than those reported by Luna-Triguerro et al.[37]

For Si-CHA, the trends are markedly different than those of Si-LTA. The non-monotonic variation of the Henry constant also translates to such trends for the adsorption enthalpy and entropy, as can be seen in Figure 8 for both *n*-alkanes and 1-alkenes. Starting with the *n*-alkanes, a linear increase in adsorption enthalpy and entropy are seen until *n*-octane, followed by a slight decrease for both properties, and finally, an increase again for *n*-undecane.

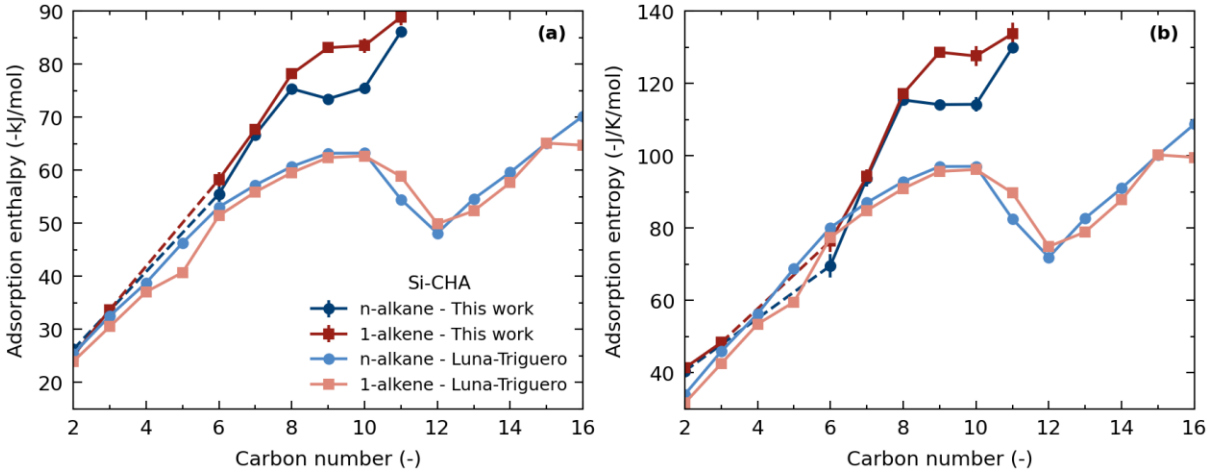


Figure 8: (a) Adsorption enthalpy and (b) adsorption entropy at zero coverage in function of the carbon number for *n*-alkanes and 1-alkenes experimentally obtained in this work (Si-CHA) and by Luna-Triguero et al.[37] via simulations (Si-CHA). Dashed lines are added to enhance the visualization and compensating for missing data due to mass transfer limitations. Standard deviation is given for *n*-alkane and 1-alkene data obtained in this work.

The length of a *n*-hexane molecule and the largest internal diameter of the CHA-cage are similar (~10 Å[83]), and studies have suggested that starting from *n*-hexane, chains have to deviate from an all-trans configuration and coil up to fit inside cage[15,59]. The apparent increase in slope of the adsorption entropy with carbon number for C_6-C_8 compared to C_2-C_6 may be an

indication of this (Figure 8b and highlighted in Figure S26). When moving from *n*-octane to *n*-nonane, the preceding linear increase in both adsorption enthalpy and entropy is disrupted by a small drop. In the range of C_9-C_{10} strong coiling or protrusion is expected which introduce repulsive interactions.

Going from *n*-decane to *n*-undecane, the adsorption enthalpy increases again at the same rate as in the C_6-C_8 range (10-11 kJ/mol slope, indicated in Figure S27). This behaviour is rationalized as follows: Once the chain has passed the pore window and is spanning over two adjacent CHA-cages, the chain can fill the second cage unconstrained as the enthalpic and entropic cost of the pore window has been paid. These results seem to agree with previous experimental and computational studies which suggest that starting from *n*-hexane chain coiling occurs, and that a coiled-chain configuration is adapted for *n*-alkanes in chabazites[15,37,38,59].

Similar behaviour is now experimentally observed for 1-alkenes in this work. Similar experimental trends in adsorption enthalpy and entropy as for the *n*-alkanes up to C_8 emerge from Figure 8. However, in contrast to the *n*-alkanes, both thermodynamic properties still increase for the 1-alkenes until 1-nonene (versus *n*-octane) and only go through a minimum in 1-decene (versus *n*-nonane). One could expect that the same number of methyl groups fit inside the CHA cage for 1-alkenes and *n*-alkanes, suggesting a different adsorption mechanism must be occurring for both homologous series in the C_9-C_{10} range. Here we hypothesize that the terminal methylidene group of 1-alkenes can reside in the pore window, allowing for different adsorption configurations within the cage, compared to the *n*-alkanes. In addition, the rigidity (or flexibility) of the double bond differs from that of a single bond. However, further investigation is necessary to unravel the exact adsorption mechanism, as inverse gas chromatography is a macroscopic technique and cannot provide direct evidence of the location of the adsorption within the crystal, for example such as a thin outer layer with different properties than the bulk crystal. In addition, non-dynamic measurements of small and

large hydrocarbons would be useful to confirm unambiguously that equilibrium is reached faster for large hydrocarbons than for smaller hydrocarbons, as discussed in Section 1.

Our results are compared to the available literature data on *n*-alkane and 1-alkene adsorption. The adsorption enthalpy and entropy of Figure 8 are compared to simulations by Luna-Triguero et al.[37], and some important similarities and differences between the datasets can be observed. Our observations demonstrate that cage nestling effects are present for hydrocarbons in Si-CHA, which is consistent with the computational study of Luna-Triguero et al.[37] However, our experimental results show that the cage nestling effects occur for smaller chains and less drastic than anticipated by the computational study. Our adsorption enthalpies and entropies are in good agreement up to C_6, even though not all components could be measured for carbon numbers below 6. However, we observe a modest minimum at C_9-C_{10}, while simulations predict a large drop to a minimum at C_{12}. A possible explanation is that chain coiling is not as effective as expected in the simulations, and protrusion occurs at shorter chain lengths, yet this requires further investigation.

4. Conclusions

Inverse gas chromatography experiments with 1-alkanes and *n*-alkanes revealed that small hydrocarbons ($<C_6$) with two successive single bonds experience slow mass transfer due to the narrow diameter of the 8r windows of Si-CHA and Si-LTA. In contrast, molecules with alternating single and double bonds gave more Gaussian-like peaks suggesting these can pass more rapidly through the pore windows. The extent of this effect decreased with increasing carbon numbers on both materials, potentially due to the longer molecule's ability to compensate the window's energy barrier by more interactions outside of the pore window.

Henry constants of *n*-alkanes and 1-alkenes up to C_{12} on Si-LTA and Si-CHA were measured at multiple temperatures (up to 330°C) and flowrates. In addition, a thermodynamical analysis using the adsorption enthalpy and entropy was performed, allowing to gain deeper

understanding of the adsorption process. The Henry constants of the hydrocarbons on Si-LTA showed a typical monotonous increase with carbon number up to C_{12}, and limited differences were observed between the adsorption enthalpies and entropies of *n*-alkanes and 1-alkenes.

Si-CHA, with its smaller cage size, exhibited a remarkable non-monotonous increase in the Henry constants, adsorption enthalpy, and entropy due to cage nestling effects. These effects occur when the molecule becomes too big for a single cage, and protrudes the pore window into an adjacent cage, and adsorbs in two cages. Typically only experimentally observed for *n*-alkanes, these effects are reported here to occur for 1-alkenes as well. Comparison of our experimental adsorption enthalpies and entropies with computational studies showed substantial differences in the magnitude and length of the transition region, as well as significant differences in adsorption enthalpy and entropy differences between *n*-alkanes and 1-alkenes.

Our observations shed light on the mass transfer limitations and cage effects that affect *n*-alkanes and 1-alkenes in pure-silica small-pore zeolites, and can contribute to a better fundamental understanding of adsorption and catalysis processes encountering these hydrocarbons. Furthermore, it provides experimental data for validating future studies on Si-CHA and Si-LTA.

Supporting information

Description and results of zeolite synthesis and characterization; Computational model; Derivation of adsorption entropy; Henry regime validation; Complementary chromatograms and van't Hoff plots of *n*-alkanes and 1-alkenes; Additional analysis; Tabulated adsorption enthalpies and pre-exponential factors at zero coverage; Tabulated Henry constants of *n*-alkanes and 1-alkenes.

Acknowledgments

N. De Witte, S. Robijns, M. Dusselier, and T.R.C. Van Assche acknowledge support from Research Foundation – Flanders (FWO Vlaanderen) through grant G085220N. SACHEM is explicitly thanked for providing the organic structure directing agent (TmAdamOH).

Declaration of competing interest

The authors declare that they have no known competing financial interests or personal relationships that could have appeared to influence the work reported in this paper.

References

(1) Dusselier, M.; Davis, M. E. Small-Pore Zeolites: Synthesis and Catalysis. *Chemical Reviews* **2018**, *118* (11), 5265–5329. https://doi.org/10.1021/acs.chemrev.7b00738.

(2) Pérez-Botella, E.; Valencia, S.; Rey, F. Zeolites in Adsorption Processes: State of the Art and Future Prospects. *Chemical Reviews* **2022**, *122* (24), 17647–17695. https://doi.org/10.1021/acs.chemrev.2c00140.

(3) Ivanushkin, G.; Dusselier, M. Engineering Lewis Acidity in Zeolite Catalysts by Electrochemical Release of Heteroatoms during Synthesis. *Chem. Mater.* **2023**, *35* (13), 5049–5058. https://doi.org/10.1021/acs.chemmater.3c00552.

(4) Kärger, J.; Ruthven, D. M.; Theodorou, D. N. *Diffusion in Nanoporous Materials*; Wiley, 2012; Vol. 1.

(5) Davis, M. E. The Quest For Extra-Large Pore, Crystalline Molecular Sieves. *Chem. Eur. J.* **1997**, *3* (11), 1745–1750. https://doi.org/10.1002/chem.19970031104.

(6) Maes, M.; Alaerts, L.; Vermoortele, F.; Ameloot, R.; Couck, S.; Finsy, V.; Denayer, J. F. M.; De Vos, D. E. Separation of C5-Hydrocarbons on Microporous Materials: Complementary Performance of MOFs and Zeolites. *J. Am. Chem. Soc.* **2010**, *132* (7), 2284–2292. https://doi.org/10.1021/ja9088378.

(7) Claessens, B.; Cousin-Saint-Remi, J.; Denayer, J. F. M. Efficient Downstream Processing of Renewable Alcohols Using Zeolite Adsorbents. In *New Developments in Adsorption/Separation of Small Molecules by Zeolites*; Valencia, S., Rey, F., Eds.; Structure and Bonding; Springer International Publishing: Cham, 2020; pp 85–119. https://doi.org/10.1007/430_2020_68.

(8) Baerlocher, Ch.; McCusker, L. B. *Database of Zeolite Structures*. http://www.iza-structure.org/databases/ (accessed 2022-10-01).

(9) Boal, B. W.; Schmidt, J. E.; Deimund, M. A.; Deem, M. W.; Henling, L. M.; Brand, S. K.; Zones, S. I.; Davis, M. E. Facile Synthesis and Catalysis of Pure-Silica and Heteroatom LTA. *Chem. Mater.* **2015**, *27* (22), 7774–7779. https://doi.org/10.1021/acs.chemmater.5b03579.

(10) Ruthven, D. M.; Reyes, S. C. Adsorptive Separation of Light Olefins from Paraffins. *Microporous and Mesoporous Materials* **2007**, *104* (1–3), 59–66. https://doi.org/10.1016/J.MICROMESO.2007.01.005.

(11) Tan, X.; Robijns, S.; Thür, R.; Ke, Q.; De Witte, N.; Lamaire, A.; Li, Y.; Aslam, I.; Van Havere, D.; Donckels, T.; Van Assche, T.; Van Speybroeck, V.; Dusselier, M.; Vankelecom, I. Truly Combining the Advantages of Polymeric and Zeolite Membranes for Gas Separations. *Science* **2022**, *378* (6625), 1189–1194. https://doi.org/10.1126/science.ade1411.

(12) Ferri, P.; Li, C.; Paris, C.; Rodríguez-Fernández, A.; Moliner, M.; Boronat, M.; Corma, A. The Limits of the Confinement Effect Associated to Cage Topology on the Control of the MTO Selectivity. *ChemCatChem* **2021**, *13* (6), 1578–1586. https://doi.org/10.1002/cctc.202001760.

(13) Tian, P.; Wei, Y.; Ye, M.; Liu, Z. Methanol to Olefins (MTO): From Fundamentals to Commercialization. *ACS Catal.* **2015**, *5* (3), 1922–1938. https://doi.org/10.1021/acscatal.5b00007.

(14) Paolucci, C.; Parekh, A. A.; Khurana, I.; Di Iorio, J. R.; Li, H.; Caballero, J. D. A.; Shih, A. J.; Anggara, T.; Delgass, W. N.; Miller, J. T.; Ribeiro, F. H.; Gounder, R.; Schneider, W. F. Catalysis in a Cage: Condition-Dependent Speciation and Dynamics of Exchanged Cu Cations in SSZ-13 Zeolites. *J. Am. Chem. Soc.* **2016**, *138* (18), 6028–6048. https://doi.org/10.1021/jacs.6b02651.

(15) Daems, I.; Singh, R.; Baron, G.; Denayer, J. Length Exclusion in the Adsorption of Chain Molecules on Chabazite Type Zeolites. *Chemical Communications* **2007**, No. 13, 1316–1318. https://doi.org/10.1039/b615661d.

(16) Ronda-Lloret, M.; Rothenberg, G.; Shiju, N. R. A Critical Look at Direct Catalytic Hydrogenation of Carbon Dioxide to Olefins. *ChemSusChem* **2019**, *12* (17), 3896–3914. https://doi.org/10.1002/cssc.201900915.

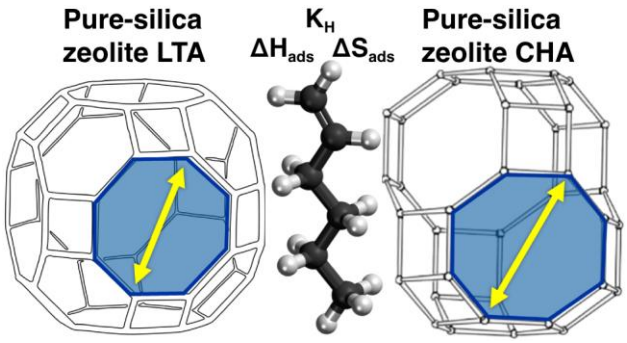
(17) Hedin, N.; DeMartin, G. J.; Strohmaier, K. G.; Reyes, S. C. PFG NMR Self-Diffusion of Propylene in ITQ-29, CaA and NaCaA: Window Size and Cation Effects. *Microporous and Mesoporous Materials* **2007**, *98* (1–3), 182–188. https://doi.org/10.1016/j.micromeso.2006.08.017.
(18) Benchaabane, M. E. A.; Trierweiler Gonçalves, G.; Bloch, E.; Paillaud, J. L.; Daou, T. J.; Bourrelly, S.; Chaplais, G.; Llewellyn, P. L. An Initial Evaluation of the Thermodynamic or Kinetic Separation Performance of Cation-Exchanged LTA Zeolites for Mixtures of Propane and Propylene. *Microporous and Mesoporous Mater.* **2022**, *344*, 112211. https://doi.org/10.1016/j.micromeso.2022.112211.
(19) Dusselier, M.; Deimund, M. A.; Schmidt, J. E.; Davis, M. E. Methanol-to-Olefins Catalysis with Hydrothermally Treated Zeolite SSZ-39. *ACS Catal.* **2015**, *5* (10), 6078–6085. https://doi.org/10.1021/acscatal.5b01577.
(20) Zones, S. I. Zeolite SSZ-13 and Its Method of Preparation. US4544538A, October 1, 1985. https://patents.google.com/patent/US4544538A/en (accessed 2023-04-25).
(21) Díaz-Cabañas, M.-J.; Barrett, P. A. Synthesis and Structure of Pure SiO2 Chabazite: The SiO2 Polymorph with the Lowest Framework Density. *Chem. Commun.* **1998**, No. 17, 1881–1882. https://doi.org/10.1039/a804800b.
(22) Corma, A.; Rey, F.; Rius, J.; Sabater, M. J.; Valencia, S. Supramolecular Self-Assembled Molecules as Organic Directing Agent for Synthesis of Zeolites. *Nature* **2004**, *431* (7006), 287–290. https://doi.org/10.1038/nature02909.
(23) Jo, D.; Ryu, T.; Park, G. T.; Kim, P. S.; Kim, C. H.; Nam, I.-S.; Hong, S. B. Synthesis of High-Silica LTA and UFI Zeolites and NH3–SCR Performance of Their Copper-Exchanged Form. *ACS Catal.* **2016**, *6* (4), 2443–2447. https://doi.org/10.1021/acscatal.6b00489.
(24) Palomino, M.; Cantín, A.; Corma, A.; Leiva, S.; Rey, F.; Valencia, S. Pure Silica ITQ-32 Zeolite Allows Separation of Linear Olefins from Paraffins. *Chemical Communications* **2007**, No. 12, 1233–1235. https://doi.org/10.1039/b700358g.
(25) Gehre, M.; Guo, Z.; Rothenberg, G.; Tanase, S. Sustainable Separations of C4-Hydrocarbons by Using Microporous Materials. *ChemSusChem* **2017**, *10* (20), 3947–3963. https://doi.org/10.1002/cssc.201700657.
(26) Castly, G. L.; Hall, R. B.; Reyes, S. C.; Reynolds, R. P.; Strohmaier, K. G. Separation of 1-Butene from C4 Feed Streams, 2006.
(27) Reyes, S. C.; Krishnan, V. V.; DeMartin, G. J.; Sinfelt, J. H.; Strohmaier, K. G.; Santiesteban, J. G. Separation of Propylene from Hydrocarbon Mixtures, 2004.
(28) Reyes, S. C.; Venkatesan, K. V.; DeMartin, G. J.; Sinfelt, J. H.; Strohmaier, K. G.; Santiesteban, J. G. Separation of Propylene and Dimethylether from Hydrocarbon Mixtures, 2004.
(29) Reyes, S. C.; Olson David H.; Liu, H.; Strohmaier, K. G.; Santiesteban, J. G. Light Hydrocarbon Separation Using 8-Member Ring Zeolites, 2008.
(30) Olson, D. H. Light Hydrocarbon Separation Using 8-Member Ring Zeolites, 2002.
(31) Olson, D. H.; Camblor, M. A.; Villaescusa, L. A.; Kuehl, G. H. Light Hydrocarbon Sorption Properties of Pure Silica Si-CHA and ITQ-3 and High Silica ZSM-58. *Microporous and Mesoporous Materials* **2004**, *67* (1), 27–33. https://doi.org/10.1016/j.micromeso.2003.09.025.
(32) Olson, D. H.; Yang, X.; Camblor, M. A. ITQ-12: A Zeolite Having Temperature Dependent Adsorption Selectivity and Potential for Propene Separation. *Journal of Physical Chemistry B* **2004**, *108* (30), 11044–11048. https://doi.org/10.1021/jp040216d.
(33) Zhu, W.; Kapteijn, F.; Moulijn, J. A.; Jansen, J. C. Selective Adsorption of Unsaturated Linear C4 Molecules on the All- Silica DD3R. *Physical Chemistry Chemical Physics* **2000**, *2* (8), 1773–1779. https://doi.org/10.1039/a909812g.
(34) Gücüyener, C.; Van Den Bergh, J.; Joaristi, A. M.; Magusin, P. C. M. M.; Hensen, E. J. M.; Gascon, J.; Kapteijn, F. Facile Synthesis of the DD3R Zeolite: Performance in the Adsorptive Separation of Buta-1,3-Diene and but-2-Ene Isomers. *Journal of Materials Chemistry* **2011**, *21* (45), 18386–18397. https://doi.org/10.1039/c1jm13671b.

(35) Krishna, R.; Van Baten, J. M. A Molecular Dynamics Investigation of the Diffusion Characteristics of Cavity-Type Zeolites with 8-Ring Windows. *Microporous and Mesoporous Materials* **2011**, *137* (1–3), 83–91. https://doi.org/10.1016/j.micromeso.2010.08.026.
(36) Hedin, N.; DeMartin, G. J.; Roth, W. J.; Strohmaier, K. G.; Reyes, S. C. PFG NMR Self-Diffusion of Small Hydrocarbons in High Silica DDR, CHA and LTA Structures. *Microporous and Mesoporous Materials* **2008**, *109* (1–3), 327–334. https://doi.org/10.1016/j.micromeso.2007.05.007.
(37) Luna-Triguero, A.; Vicent-Luna, J. M.; Dubbeldam, D.; Gómez-Álvarez, P.; Calero, S. Understanding and Exploiting Window Effects for Adsorption and Separations of Hydrocarbons. *The Journal of Physical Chemistry C* **2015**, *119* (33), 19236–19243. https://doi.org/10.1021/acs.jpcc.5b05597.
(38) Dubbeldam, D.; Smit, B. Computer Simulation of Incommensurate Diffusion in Zeolites: Understanding Window Effects. *Journal of Physical Chemistry B* **2003**, *107* (44), 12138–12152. https://doi.org/10.1021/jp040003o.
(39) Findley, J. M.; Boulfelfel, S. E.; Fang, H.; Muraro, G.; Ravikovitch, P. I.; Sholl, D. S. A Transferable Force Field for Predicting Adsorption and Diffusion of Hydrocarbons and Small Molecules in Silica Zeolites with Coupled-Cluster Accuracy. *Journal of Physical Chemistry C* **2021**, *125* (15), 8418–8429. https://doi.org/10.1021/acs.jpcc.1c00943.
(40) Gribov, E. N.; Sastre, G.; Corma, A. Influence of Pore Dimension and Sorption Configuration on the Heat of Sorption of Hexane on Monodimensional Siliceous Zeolites. *Journal of Physical Chemistry B* **2005**, *109* (50), 23794–23803. https://doi.org/10.1021/jp052462a.
(41) Liu, B.; Smit, B.; Calero, S. Evaluation of a New Force Field for Describing the Adsorption Behavior of Alkanes in Various Pure Silica Zeolites. *Journal of Physical Chemistry B* **2006**, *110* (41), 20166–20171. https://doi.org/10.1021/jp064413j.
(42) Liu, B.; Smit, B.; Rey, F.; Valencia, S.; Calero, S. A New United Atom Force Field for Adsorption of Alkenes in Zeolites. *Journal of Physical Chemistry C* **2008**, *112* (7), 2492–2498. https://doi.org/10.1021/jp075809d.
(43) Boulfelfel, S. E.; Ravikovitch, P. I.; Sholl, D. S. Modeling Diffusion of Linear Hydrocarbons in Silica Zeolite LTA Using Transition Path Sampling. *Journal of Physical Chemistry C* **2015**, *119* (27), 15643–15653. https://doi.org/10.1021/acs.jpcc.5b01633.
(44) Boulfelfel, S. E.; Ravikovitch, P. I.; Koziol, L.; Sholl, D. S. Improved Hill-Sauer Force Field for Accurate Description of Pores in 8-Ring Zeolites. *Journal of Physical Chemistry C* **2016**, *120* (26), 14140–14148. https://doi.org/10.1021/acs.jpcc.6b03674.
(45) Combariza, A. F.; Sastre, G.; Corma, A. Molecular Dynamics Simulations of the Diffusion of Small Chain Hydrocarbons in 8-Ring Zeolites. *Journal of Physical Chemistry C* **2011**, *115* (4), 875–884. https://doi.org/10.1021/jp102262n.
(46) Sławek, A.; Vicent-Luna, J. M.; Ogorzały, K.; Valencia, S.; Rey, F.; Makowski, W.; Calero, S. Adsorption of Alkanes in Zeolites LTA and FAU: Quasi-Equilibrated Thermodesorption Supported by Molecular Simulations. *Journal of Physical Chemistry C* **2019**, *123* (49), 29665–29678. https://doi.org/10.1021/acs.jpcc.9b07907.
(47) Calero, S.; Dubbeldam, D.; Krishna, R.; Smit, B.; Vlugt, T. J. H.; Denayer, J. F. M.; Martens, J. A.; Maesen, T. L. M. Understanding the Role of Sodium during Adsorption: A Force Field for Alkanes in Sodium-Exchanged Faujasites. *Journal of the American Chemical Society* **2004**, *126* (36), 11377–11386. https://doi.org/10.1021/ja0476056.
(48) Smit, B.; Maesen, T. L. M. Molecular Simulations of Zeolites: Adsorption, Diffusion, and Shape Selectivity. *Chem. Rev.* **2008**, *108* (10), 4125–4184. https://doi.org/10.1021/cr8002642.
(49) Jeffroy, M.; Nieto-Draghi, C.; Boutin, A. New Molecular Simulation Method To Determine Both Aluminum and Cation Location in Cationic Zeolites. *Chemistry of Materials* **2017**, *29* (2), 513–523. https://doi.org/10.1021/acs.chemmater.6b03011.
(50) Robijns, S.; Devos, J.; Donckels, T.; de Oliveira-Silva, R.; De Witte, N.; Sakellariou, D.; Van Assche, T. R. C.; Dusselier, M. Steering Interzeolite Conversion with Alkali Metal Cations: Lithium

Maximizes Al Proximity in SSZ-13 Zeolite Genesis. *Crystal Growth and Design* **2023**, *23* (1), 289–299. https://doi.org/10.1021/acs.cgd.2c01009.
(51) Findley, J. M.; Ravikovitch, P. I.; Sholl, D. S. The Effect of Aluminum Short-Range Ordering on Carbon Dioxide Adsorption in Zeolites. *Journal of Physical Chemistry C* **2018**, *122* (23), 12332–12340. https://doi.org/10.1021/acs.jpcc.8b03475.
(52) Ter Horst, J. H.; Bromley, S. T.; Van Rosmalen, G. M.; Jansen, J. C. Molecular Modelling of the Transport Behaviour of C3 and C4 Gases through the Zeolite DD3R. *Microporous and Mesoporous Materials* **2002**, *53* (1–3), 45–57. https://doi.org/10.1016/S1387-1811(02)00323-2.
(53) Maesen, T. L. M.; Beerdsen, E.; Calero, S.; Dubbeldam, D.; Smit, B. Understanding Cage Effects in the N-Alkane Conversion on Zeolites. *Journal of Catalysis* **2006**, *237* (2), 278–290. https://doi.org/10.1016/j.jcat.2005.11.007.
(54) Dubbeldam, D.; Calero, S.; Maesen, T. L. M.; Smit, B. Incommensurate Diffusion in Confined Systems. *Physical Review Letters* **2003**, *90* (24), 4. https://doi.org/10.1103/PhysRevLett.90.245901.
(55) Dubbeldam, D.; Calero, S.; Maesen, T. L. M.; Smit, B. Understanding the Window Effect in Zeolite Catalysis. *Angewandte Chemie - International Edition* **2003**, *42* (31), 3624–3626. https://doi.org/10.1002/anie.200351110.
(56) Denayer, J. F.; Baron, G. V.; Martens, J. A.; Jacobs, P. A. Chromatographic Study of Adsorption of N-Alkanes on Zeolites at High Temperatures. *Journal of Physical Chemistry B* **1998**, *102* (17), 3077–3081. https://doi.org/10.1021/jp972328t.
(57) Arik, I. C.; Denayer, J. F.; Baron, G. V. High-Temperature Adsorption of n-Alkanes on ZSM-5 Zeolites: Influence of the Si/Al Ratio and the Synthesis Method on the Low-Coverage Adsorption Properties. *Microporous and Mesoporous Materials* **2003**, *60* (1–3), 111–124. https://doi.org/10.1016/S1387-1811(03)00332-9.
(58) Jobic, H.; Méthivier, A. Intracrystalline Diffusion in Zeolites Studied by Neutron Scattering Techniques. *Oil & Gas Science and Technology* **2005**, *60* (5), 815–830. https://doi.org/10.2516/ogst:2005058.
(59) Denayer, J. F. M.; Devriese, L. I.; Couck, S.; Martens, J.; Singh, R.; Webley, P. A.; Baron, G. V. Cage and Window Effects in the Adsorption of N-Alkanes on Chabazite and SAPO-34. *Journal of Physical Chemistry C* **2008**, *112* (42), 16593–16599. https://doi.org/10.1021/jp804349v.
(60) Jobic, H.; Méthivier, A.; Ehlers, G.; Farago, B.; Haeussler, W. Accelerated Diffusion of Long-Chain Alkanes between Nanosized Cavities. *Angewandte Chemie - International Edition* **2004**, *43* (3), 364–366. https://doi.org/10.1002/anie.200352691.
(61) Brandani, S.; Ruthven, D. M.; Caro, J.; Jobic, H.; Krause, C.; Kärger, J.; Möller, A.; Staudt, R.; Yang, X. A Remarkable Non-Monotonical Chain-Length Dependence: Diffusion of n-Alkanes in Zeolites LTA; 2005.
(62) Ruthven, D. M. Comment on "Computer Simulation of Incommensurate Diffusion in Zeolites: Understanding Window Effects." *Journal of Physical Chemistry B* **2004**, *108* (41), 16328–16329. https://doi.org/10.1021/jp040003o.
(63) Dubbeldam, D.; Maesen, T. L. M.; Smit, B. Reply to the Comment on "Computer Simulation of Incommensurate Diffusion in Zeolites: Understanding Window Effects." *Journal of Physical Chemistry B* **2004**, *108* (41), 16330. https://doi.org/10.1021/jp040003o.
(64) Krishna, R.; Van Baten, J. M. Influence of Adsorption Thermodynamics on Guest Diffusivities in Nanoporous Crystalline Materials. *Physical Chemistry Chemical Physics* **2013**, *15* (21), 7994–8016. https://doi.org/10.1039/c3cp50449b.
(65) Beerdsen, E.; Dubbeldam, D.; Smit, B. Understanding Diffusion in Nanoporous Materials. *Physical Review Letters* **2006**, *96* (4), 1–4. https://doi.org/10.1103/PhysRevLett.96.044501.
(66) Gorring, R. L. Diffusion of Normal Paraffins in Zeolite T: Occurrence of Window Effect. *Journal of Catalysis* **1973**, *31* (1), 13–26. https://doi.org/10.1016/0021-9517(73)90265-0.

(67) Ruthven, D. M. The Window Effect in Zeolitic Diffusion. *Microporous and Mesoporous Materials* **2006**, *96* (1), 262–269. https://doi.org/10.1016/j.micromeso.2006.07.005.
(68) Kärger, J.; Ruthven, D. M.; Valiullin, R. Diffusion in Nanopores: Inspecting the Grounds. *Adsorption* **2021**, *27* (3), 267–281. https://doi.org/10.1007/s10450-020-00277-6.
(69) Daems, I.; Baron, G. V.; Punnathanam, S.; Snurr, R. Q.; Denayer, J. F. M. Molecular Cage Nestling in the Liquid-Phase Adsorption of n-Alkanes in 5A Zeolite. *Journal of Physical Chemistry C* **2007**, *111* (5), 2191–2197. https://doi.org/10.1021/jp0668145.
(70) Maghsoudi, H.; Abdi, H.; Aidani, A. Temperature- and Pressure-Dependent Adsorption Equilibria and Diffusivities of Propylene and Propane in Pure-Silica Si-CHA Zeolite. *Industrial and Engineering Chemistry Research* **2020**, *59* (4), 1682–1692. https://doi.org/10.1021/acs.iecr.9b05451.
(71) Kang, J. H.; Alshafei, F. H.; Zones, S. I.; Davis, M. E. Cage-Defining Ring: A Molecular Sieve Structural Indicator for Light Olefin Product Distribution from the Methanol-to-Olefins Reaction. *ACS Catal.* **2019**, *9* (7), 6012–6019. https://doi.org/10.1021/acscatal.9b00746.
(72) Ruthven, D. M. *Principles of Adsorption & Adsorption Processes*; John Wiley & Sons, 1984.
(73) Food, U. S.; Administration, D. Center for Drug Evaluation and Research, US Food and Drug Administration. In *Eightieth Meeting of the Cardiovascular and Renal Drugs Advisory Committee*; US Department of Health and Human Services Washington, DC, 1997.
(74) Fornstedt, T.; Zhong, G.; Guiochon, G. Peak Tailing and Mass Transfer Kinetics in Linear Chromatography. *Journal of Chromatography A* **1996**, *741* (1), 1–12. https://doi.org/10.1016/0021-9673(96)00152-5.
(75) Gotmar, G.; Fornstedt, T.; Guiochon, G. Peak Tailing and Mass Transfer Kinetics in Linear Chromatography: Dependence on the Column Length and the Linear Velocity of the Mobile Phase. *Journal of Chromatography A* **1999**, *831* (1), 17–35. https://doi.org/10.1016/S0021-9673(98)00648-7.
(76) Ahuja, S. *Chromatography and Separation Science*; Academic Press, 2003.
(77) Maghsoudi, H. Comparative Study of Adsorbents Performance in Ethylene/Ethane Separation. *Adsorption* **2016**, *22* (7), 985–992. https://doi.org/10.1007/s10450-016-9805-x.
(78) van Deemter, J. J.; Zuiderweg, F. J.; Klinkenberg, A. Longitudinal Diffusion and Resistance to Mass Transfer as Causes of Nonideality in Chromatography. *Chemical Engineering Science* **1956**, *5* (6), 271–289. https://doi.org/10.1016/0009-2509(56)80003-1.
(79) Denayer, J. F.; Souverijns, W.; Jacobs, P. A.; Martens, J. A.; Baron, G. V. High-Temperature Low-Pressure Adsorption of Branched C_5 −C_8 Alkanes on Zeolite Beta, ZSM-5, ZSM-22, Zeolite Y, and Mordenite. *The Journal of Physical Chemistry B* **1998**, *102* (23), 4588–4597. https://doi.org/10.1021/jp980674k.
(80) Ocakoglu, R. A.; Denayer, J. F. M.; Marin, G. B.; Martens, J. A.; Baron, G. V. Tracer Chromatographic Study of Pore and Pore Mouth Adsorption of Linear and Monobranched Alkanes on ZSM-22 Zeolite. *Journal of Physical Chemistry B* **2003**, *107* (1), 398–406. https://doi.org/10.1021/jp0264533.
(81) Denayer, J. F. M.; Baron, G. V. The Confinement Factor: A Thermodynamic Parameter to Characterize Microporous Adsorbents. *Adsorption* **2005**, *11* (1 SUPPL.), 85–90. https://doi.org/10.1007/s10450-005-5903-x.
(82) Dunitz, J. D. Win Some, Lose Some: Enthalpy-Entropy Compensation in Weak Intermolecular Interactions. *Chemistry & Biology* **1995**, *2* (11), 709–712. https://doi.org/10.1016/1074-5521(95)90097-7.
(83) De Meyer, K. M. A.; Chempath, S.; Denayer, J. F. M.; Martens, J. A.; Snurr, R. Q.; Baron, G. V. Packing Effects in the Liquid-Phase Adsorption of C5- C22 n-Alkanes on ZSM-5. *Journal of Physical Chemistry B* **2003**, *107* (39), 10760–10766. https://doi.org/10.1021/jp0354144.

TOC Graphic


Pure-silica
zeolite LTA
K_H
ΔH_{ads} ΔS_{ads}
Pure-silica
zeolite CHA